

# Identification of resting state brain networks from EEG with simultaneous MEG

Tammo Rukat, University of Oxford

**Abstract**—Functional brain networks exhibit dynamics on the sub-second temporal scale and are often assumed to embody the physiological substrate of cognitive processes. Here we analyse the temporal and spatial dynamics of these states, as measured by EEG, with a Hidden Markov model and compare this approach to classical EEG microstate analysis. We find dominating state lifetimes of 100–150 ms for both approaches and the state topographies show obvious similarities. However, they also feature distinct spatial and especially temporal properties. We hypothesise that these differences carry physiological meaningful information and originate from patterns in the data that the HMM is able to integrate while the microstate analysis is not. This is supported by a consistently high pairwise correlation of the temporal evolution of EEG microstates which is not observed for the HMM states and which seems unlikely to be a good description of the underlying physiology.

We use a general linear model to combine EEG state time courses with the power envelopes of simultaneously acquired MEG data. This highlights the similarities between both methods and improves our spatial understanding of the activation patterns. However, a correspondence to known RSNs is largely missing for both approaches. The multimodal analysis thus fails to provide any further clear evidence for our hypothesis.

## I. INTRODUCTION

TEMPORAL correlations in the spontaneous oscillatory activity of spatially distinct neuronal assemblies are a well established phenomenon described as *resting state brain networks*. RSNs exhibit functional [1] and clinical [2, 3, 4, 5] significance. They have first been identified based on blood-oxygen levels measured through *functional MRI* [6, 7]. While fMRI is limited in its temporal resolution and captures only slow oscillations with frequencies below 0.1 Hz, it features a high spatial resolution down to 1mm. In contrast, *electroencephalography* (EEG) and *magnetoencephalography* (MEG) are techniques that provide a more direct measure of the electrical activity in the brain [8, 9]. The MEG signal originates from magnetic fields that are induced by the current flow through the dendrites of pyramidal neurons. Conversely, EEG measures difference in electric potentials directly on the scalp. Both techniques capture high frequency oscillations on the millisecond timescale that is most relevant for the characterisation of cognitive processes. Therefore MEG and EEG are suitable tools to characterise the electrophysiological basis of RSNs [10, 11]. Notably, the same resting state patterns

This work was jointly supervised by Mark Woolrich, Stephen Smith (University of Oxford), Markus von Kienlin and Andreas Bruns (Hoffmann-La Roche). It was carried out within the EPSRC funded Systems Approaches to Biomedical Sciences Centre for Doctoral Training, where TR is a doctoral student.

For correspondence please visit: <https://tammor.github.io>.

Handed in for assessment October 9, 2015.

can be observed across the different time scales of fMRI and M/EEG, which is made conceivable by the dynamics of brain states being scale free across the relevant regime [12, 13, 14]. The more direct nature of the MEG measurement facilitates a projection of the signal into source space, which is accomplished by solving an inverse problem, an example of which is *beamforming* [15, 16, 17]. As opposed to this, EEG signals are often analysed as a projection onto the 2D axial plane.

Here, we apply a hidden Markov Model (HMM) [18, 19, 20] to the power envelope of EEG and MEG signals in sensor space, in order to identify quasi-stable networks of correlated activation that the signal is likely to have emerged from. The aim of this study is to investigate the HMM's potential as an alternative or complementary method to classical EEG microstate analysis. We compare their spatial and temporal characteristics and subsequently combine the results with simultaneously recorded MEG data.

We proceed in the introduction by briefly discussing classical EEG microstate analysis, as well as multimodal approaches to the investigation of resting state networks. Thereupon section II describes the data acquisition and preprocessing, before the classical microstate analysis is delineated in section III. Section IV introduces the Hidden Markov model, which is then separately applied to EEG and MEG measurements. Quasi-stable EEG topographies, as identified by the HMM, are compared to EEG microstates in section V and eventually both methods are combined with the simultaneously acquired MEG measurement, as described in section VI. We close with a discussion and concluding remarks in section VII.

## A. EEG microstates

A commonly applied procedure to investigate the dynamics of global electric field configurations based on EEG recordings is known as *EEG microstates* [21, 22, 23, 24]. In classical microstate analysis, the EEG signal is thought of as a sequence of a limited number of quasi-stable EEG topographies, each defining a microstate. These are inferred based on the EEG topographies at local maxima of the global field power (GFP), which is given by the sum squared difference between all electrode potentials  $V_i$  and the mean potential  $\bar{V}$ .

$$\text{GFP}(t) = \sqrt{\frac{1}{n} \sum_i V_i(t) - \bar{V}(t)} \quad (1)$$

Topographies at the GFP maxima are of particular interest because they feature the highest signal-to-noise ratio [25].

Additionally, it is sometimes argued that the number of considered topographies needs to be limited for sake of computational feasibility of the subsequent analysis [26]. The selected topographies are subject to a clustering procedure that aims to determine a fixed number of states, reflecting typical topographies. Traditionally this is achieved by an iterative procedure [27], while K-means clustering or more sophisticated hierarchical clustering methods [28, 8] have become the current standard. More recently independent component analysis has been proposed to find temporally independent clusters [29]. Classical microstate analysis usually limits itself to 4 clusters that have been repeatedly observed to explain most variance in the data and that usually feature topographies similar to those shown in fig. 1. Time courses can then be derived under

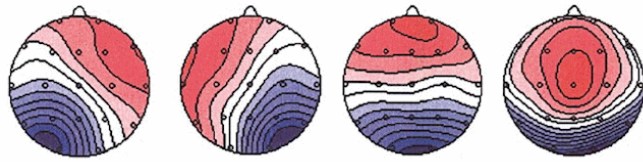


**Fig. 1: Classical EEG microstates** – Frequently microstate analysis is performed with a fixed number of four clusters, yielding topographies that appear similar. Shown are the normalised mean equipotential contour maps across 496 subjects, where red and blue code for opposite polarity (adopted from [22]).

the assumption that the switching between mutually exclusive microstates happens only at GFP peaks. This procedure yields mean state durations of around 100 ms [23, 30]. Microstates have a variety of clinical applications, e.g. in Schizophrenia [31] and Alzheimer’s [32], where durations of and switching patterns between the four microstates are connected to the disease state. However, the extent to which they reflect topographies of physiological activation remains unclear. It should also be noted that more sophisticated techniques have been successfully applied [33].

### B. Comparing modalities

Several studies have been undertaken to investigate the electrophysiological basis of the haemodynamic oscillations from fMRI RSNs. By means of *simultaneous EEG/fMRI* recordings, significant correlations of fMRI RSNs with the EEG signal across EEG frequency bands have been revealed [34]. Furthermore it has been shown that EEG microstates represent a correlate of the known fMRI RSNs [35, 29]. Opposed to EEG/fMRI, *simultaneous MEG/fMRI* studies are technically impossible. Nevertheless, separately recorded resting state data from both modalities can be compared and clear correlations between pairwise correlations of spatially co-registered MEG and fMRI sources have been found [36]. Finally, *simultaneous MEG/EEG* measurements can be obtained and have been shown to provide clinically relevant information that can not be obtained by any of the modalities alone [37, 38].

## II. DATA ACQUISITION AND PREPROCESSING

Combined MEG and EEG data was acquired for six healthy subjects, with two sessions comprising ten minutes of data for each subject. During each session, the subjects were asked to sit still and loosely fixate on a fixation cross. MEG data was acquired using a 306 channel Elekta Neuromag system (Helsinki, Finland) comprising 102 magnetometers and 204 planar gradiometers. The data was gathered at a sampling frequency of 1000 Hz with a 0.1 Hz high-pass filter. EEG data was simultaneously acquired from 60 Ag-AgCl electrodes in an elastic cap (EASYCAP GmbH, Herrsching-Breitbrunn, Germany). Localisation of the head within the MEG helmet was achieved using three electromagnetic head position indicator (HPI) coils. By periodically energising these coils their position within the MEG sensor array was identified. Prior to data acquisition, the EEG electrodes, the HPI coil locations, the position of three fiducial points (the nasion, and left and right pre-auricular points), and the head shape were recorded using a three-dimensional digitiser (Polhemus Fastrack). The location of the MEG sensors were co-registered to each individual subject’s structural MRI by matching the digitised head surface to the head surface extracted from the anatomical image. Electrodes were also placed on the wrist to record the electrocardiogram (ECG), and above and below the eye to record the electrooculogram (EOG). Blinks and saccades were recorded using an Eyelink-1000 infrared eye tracker (SR Research, Osgoode, Canada).

The data was converted to SPM8<sup>1</sup> and down-sampled to 250 Hz. Upon identification based on the cardiac signal, the eye blink signal and the signal’s kurtosis and frequency spectrum, channels and periods of data that contained apparent artefacts were manually removed. Thereupon the data was decomposed into 150 independent components<sup>2</sup> and subsequently band-pass filtered into the 1–40 Hz band. To estimate the electrical activity in brain space, the processed MEG data was projected onto a 8 mm grid that spans the entire brain [39] and that were refer to as *source space*. To this end, a linearly constrained minimum variance scalar beamformer was used, that is described in detail elsewhere [15]. Power envelopes were calculated and further down sampled to 42 Hz. For group level analysis these envelopes were demeaned and variance normalised and subsequently concatenated. To ensure computational feasibility the concatenated envelopes were subject to dimensionality reduction. We use 40 principal components for the MEG and 20 principal components for the EEG data, accounting for about 70% and 95% of the variation in the data, respectively.

## III. EEG MICROSTATE ANALYSIS

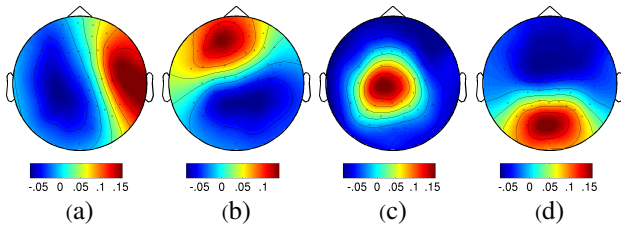
Microstates are inferred as described in section I-A. The Global field power (GFP) time course is smoothed with a Gaussian kernel with a width of 10 time steps and a standard deviation of 5 time steps, both at 42 Hz. GFP peaks are considered local maxima if all 10 surrounding values are smaller. Upon identification, the peak topographies are subject

<sup>1</sup><http://www.fil.ion.ucl.ac.uk/spm/software/spm8/>

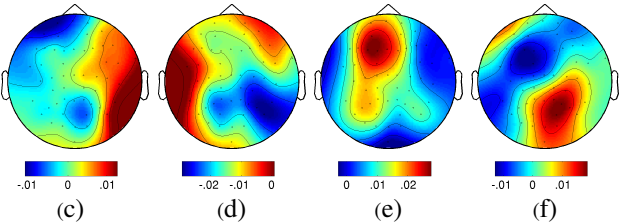
<sup>2</sup><http://research.ics.aalto.fi/ica/fastica>

to k-means clustering with a fixed number of clusters, where the objective function is the within sample correlation for each cluster. The mean distance for each topography from its assigned centroid under variation of the number of states is shown in Fig. 8 in the appendix and exhibits a steady decrease, not immediately suggesting a certain number of clusters that is particularly well supported by the data.

While the subsequent topographies are robust to changes of the parameters for smoothing and maxima identification within at least an order of magnitude, the choice of a different objective function such as the squared euclidean distance or the cosine distance leads to different topographies. Overall, the correlation measure we used generates microstate topographies that appear most similar to those found in the literature. They are shown in Fig. 2 (1). Furthermore, microstates for fixed



(1) Classical EEG microstates, identified by k-means clustering of the topographies at local maxima of the GFP. Compare to typical microstates, shown in Fig. 1.



(2) Hidden Markov states, derived with a Gaussian observation model as described in section IV. The absolute potential values vary strongly between topographies

**Fig. 2: Quasi-stable spatial EEG topographies** – Based on resting state EEG measurement for 2x10 minutes in 6 subjects. The red-blue colour coding shows opposite potentials. As opposed to the microstates, the range in potentials differs among HMM states. They are separately normalised to facilitate the comparison between modalities (see colourbars).

numbers of 2 to 12 clusters are shown in Fig. 11 in the appendix. Upon introduction of additional states, clusters split up in a mostly symmetric manner. We also investigate the microstates for each subject separately, shown in Fig. 12 in the appendix. States appear similar in most subjects with only a few exceptions. For instance the anterior activation, that appears mixed with the left lateral activation in the group microstate (a), is spread out in subject 2 and strongly restricted in subject 3. In turn, subject 2 lacks states of clear lateral activation. Interestingly right lateral activation is strongly visible in most subjects, while left lateral activation is not.

#### IV. A HIDDEN MARKOV MODEL FOR EEG AND MEG TOPOGRAPHIES

In contrast to classical microstate analysis, the hidden Markov model, as proposed here, is a generative model that describes the observations that emerge from the rapid switching between quasi-stable topographies with a Gaussian observation model. It promises to be able to capture temporal and spatial dynamics that are more closely related to the underlying brain activity than classical microstate analysis and has been successfully applied to the analysis of MEG RSNs [19]. We now briefly outline the model, of which a detailed account is given elsewhere [20].

##### A. Model derivation

At any given time  $t$  the system is in a state  $k$  out of fixed number,  $K$ , of states, denoted  $s_t$ . Each of these states is associated with a Gaussian observation model that describes the mean and covariance for every data point. With  $y_t$  denoting the vector of observation at time  $t$  we therefore write:

$$P(y_t|s_t = k, \mu_k, \Sigma_k) \sim \mathcal{N}(\mu_k, \Sigma_k). \quad (2)$$

The transition probability between states is Markovian, such that

$$\begin{aligned} P(s_t = k|s_{t-1} = k', s_{t-2} = k'', \dots) &= \\ P(s_t = k|s_{t-1} = k') &= \pi_{k,k'} \end{aligned} \quad (3)$$

where the transition probabilities from state  $k$  to  $k'$  are described by  $K \times K$  matrix  $\pi$ . The initial probability to be in state  $k$  is given by  $\pi_0$ . The full posterior likelihood is given by:

$$\begin{aligned} P(y, s, \pi_0, \pi, \mu_k, \Sigma_k) &= \\ \prod_t P(y_t|s_t, \mu_k, \Sigma_k) P(s_t|s_{t-1}, \pi) P(\pi_t) P(\pi_0) P(\mu, \Sigma) & \end{aligned} \quad (4)$$

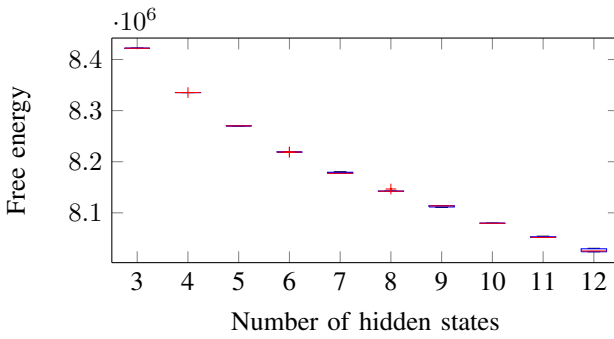
Choosing conjugate distributions for the priors,  $P(\pi_t)$ ,  $P(\pi_0)$ , and  $P(\mu, \Sigma)$  facilitates the approximation of the posterior distribution by means of variational Bayes inference [18]. To this end, the posterior distribution is approximated to factorise, such that

$$P(y, s, \pi_0, \pi, \mu_k, \Sigma_k) \approx P(y) P(s) P(\pi_0, \pi) P(\mu, \sigma) =: Q. \quad (5)$$

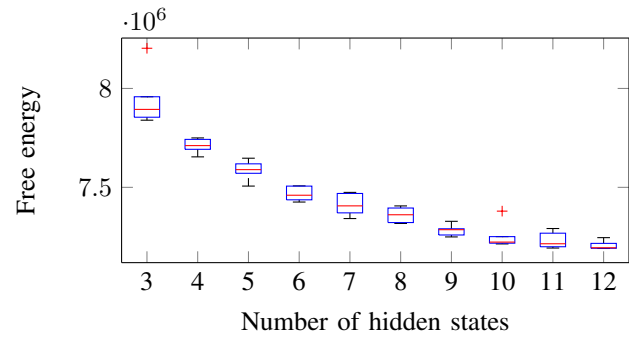
$Q$  is then determined by minimising the variational free energy [40] between the true posterior and this approximation. Up to an additive constant this free energy equals the KL divergence between the two distributions.

##### B. Application to MEG and EEG envelopes

We apply this model separately to EEG and MEG power envelopes. The number of states that is supported by the data is investigated by plotting the free energy as a function of the number of states, as shown in Fig. 3. For both, EEG and MEG data the free energy decreases steadily for larger numbers of states, which is in agreement with earlier observations by Baker and colleagues [19]. However, we base our choice of the number of states onto comparability with classical EEG



(a) From MEG power envelopes, 40 principal components.



(b) From EEG power envelopes, 20 principal components.

**Fig. 3: Free energy of the variational approximation for different numbers of hidden states** – Variational Bayes inference is repeated 10 times for every fixed number of Markov states. Inference on the MEG data exhibits a higher variability and a minimum at 4 states. As opposed to this, the free energy for the EEG inference is steadily decreasing.

microstate analysis (4 states) and with the previous study of HMM states in resting state MEG by Baker et al. [19] (8 states).

The HMM is applied to 40 principal components of the power envelopes of the acquired MEG data after parcellation into known brain regions. The resulting states are shown in Fig. 10 in the appendix. We find known activation patterns such as the visual and motor activation, as well as visual and SPL (superior parietal lobule) deactivation. We also find the default mode network with exception of the posterior cingulate cortex, which is in close agreement to the earlier observations [19]. Next, the HMM is applied to the 20 first principal components of the EEG power envelopes. State topographies are derived with a general linear model with the inferred HMM state time course as design matrix and the EEG sensor space power as response. The resulting coefficients are maps of partial correlations, shown in Fig. 2 (2). We also show the HMM states for every subject in Fig. 13 (appendix). In comparison to the microstates, commonalities with the group topographies are less apparent.

## V. COMPARISON OF EEG MICROSTATES AND MARKOV STATES

EEG microstates and EEG HMM states show clear spatial similarities. The activation is mostly limited to one specific region of the plane and both, microstate and HMM state topographies can be broadly classified as right lateral, left lateral, anterior/central, and posterior. The lateral microstates expand more into anterior areas, while the corresponding HMM states are laterally confined. Notably, the absolute range of potential differences differs between HMM states and is virtually identical between microstates.

We further compare the temporal properties of both sets of states. Similarly to the HMM state analysis, microstate time courses are obtained as partial correlation between each microstate topography and the EEG power envelope time course. The most probable state  $s_t$  at every time point is derived using the Viterbi algorithm [18]. It facilitates an estimate of the overall fractional occupancy of each state, which is similar between states and models. The relative time

spent in each HMM state (microstate) is (a): 28% (24%), (b): 26% (25%), (c): 20% (21%), (d) 25% (29%). Pairwise correlations of the full time courses are shown in Fig. 4. The

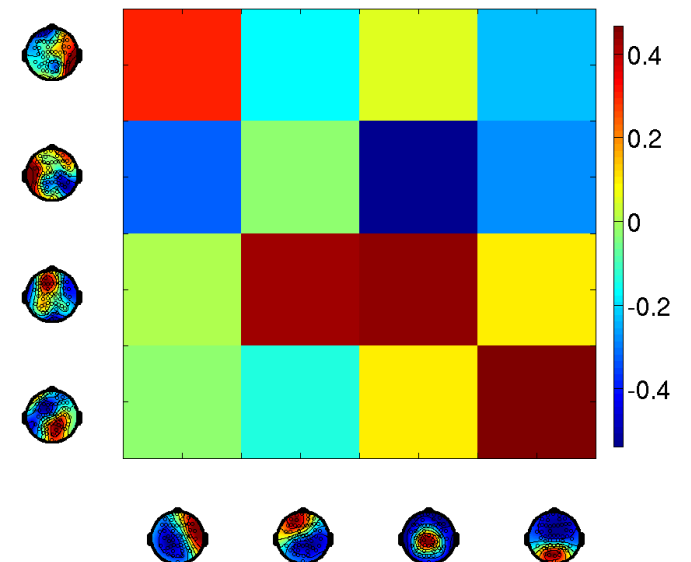


**Fig. 4: Correlation structure of microstate and HMM state time courses** – The heatmap depicts the temporal correlation of the states. With exception of the second HMM state the temporal correlation is in qualitative agreement with matching of spatially similar states.

corresponding spatial correlations are shown in Fig. 9 in the appendix. Overall, they exhibit a very similar pattern. There are however clear difference, as for instance a strong spatial correlation between microstate (b) and HMM state (b), which is not reflected in the temporal correlation. Conversely microstate (c) and HMM state (d) feature a moderately positive time course correlation, while the spatial patterns are negatively correlated.

Overall, the topographies mostly agree with the pairwise qualitative identification of states that we described above, with the exception of the left anterior microstate (b), that is more highly correlated with the anterior HMM state (c) than

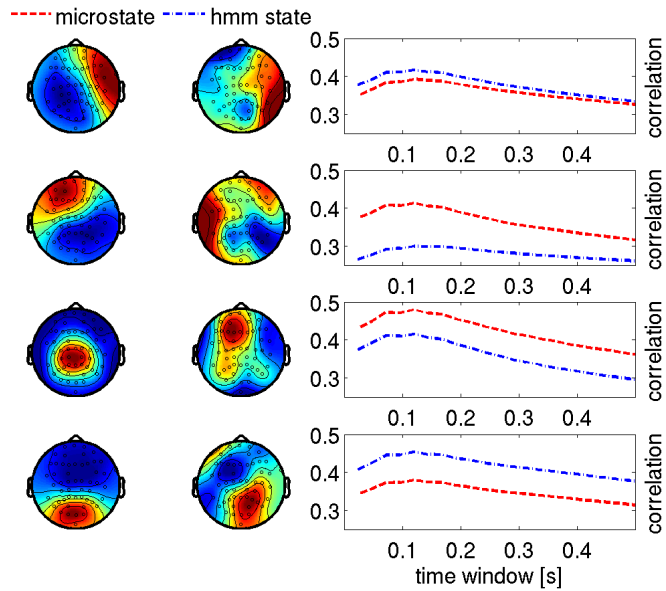


**Fig. 5: Time scale analysis of within-topography fluctuations** – The fractional occupancy time window dependency of the correlation between the microstate and HMM state time course and the envelope of the most representative EEG sensor is shown and exhibits consistent maxima around 100–150 ms. See Fig. 2 for colourbars.

with the left lateral HMM state (b). Since the time courses for the two modalities are partial correlations of the topographies with the identical envelope time courses it seems unsurprising that they are in close agreement with the spatial overlap of the topographies. However, it is clear that the temporal evolution features information complimentary to the 2D topographies. For instance, a comparison between HMM states (a) and (b) with microstate (c) shows a weak positive correlation in the first and a strongly negative correlation of the time courses in the latter case. This observation can not be inferred from the topographies alone.

To investigate the time scale of the inferred dynamics of state switching as supported by the envelope data we correlate low pass filtered versions of each state time course with the envelope fluctuation of a representative EEG sensor. We selected the sensor that has the highest correlation with the unfiltered state time course and repeated this analysis for every microstate and every HMM state varying the width of the filter. The results are shown in Fig. 5 and consistently exhibit maxima in the correlation at window width of 100–150 ms. This observation is in good agreement with results from Baker et al. [19], who identified stable periods of 100–200 ms lengths in MEG data using the same low-pass procedure, and also agrees with previous observations for EEG microstates [41]. Notably, none of the modalities shows a steadily higher correlation than the other.

## VI. COMBINED EEG AND MEG STATE TOPOGRAPHIES

Since EEG and MEG data was recorded simultaneously, the information from EEG microstates and HMM states can be

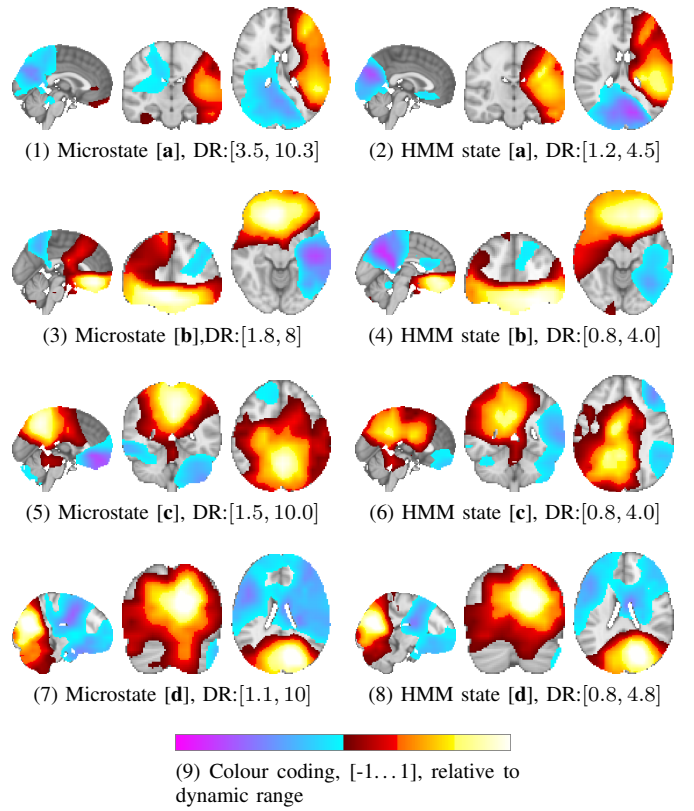


**Fig. 6: Partial correlation of MEG envelopes with EEG microstate and EEG HMM state time courses** – The dynamic range is given in multiples  $10^{-3}$  and chosen so as to highlight the similarity between the HMM and microstate regressors. Activations are therefore not directly quantitatively comparable. Compare with the microstate and HMM state topographies in Fig. 2.

combined with the temporal progression and voxel-wise spatial pattern of the MEG signal. This enables us to investigate the states of stable EEG topographies in the three dimensional MEG source space, which is achieved by calculating the partial correlation of each demeaned and variance normalized EEG state time course with the MEG source power envelopes as shown in Fig. 6.

Unsurprisingly, the topographies for corresponding EEG states appear overall similar. Those derived from HMM EEG states are slightly more confined and less prone to small noise-like activations, as for instance in the coronal plane in Fig. 6 (1) (compared to Fig. 6 (2)). Strikingly, known resting state activation patterns are not apparent. However, the combined data does provide some additional insights. For instance Fig. 6 (1) confirms a deactivation in the visual area that is visible in the corresponding HMM state but not in the corresponding microstate. Similarly Fig. 6 (3) and (4) show deactivation in the sensory cortex that can not be inferred from EEG HMM states or microstates. Again, this physiologically plausible observation is more distinct in the topographies that are based on EEG HMM state, than in those that are based on EEG microstates.

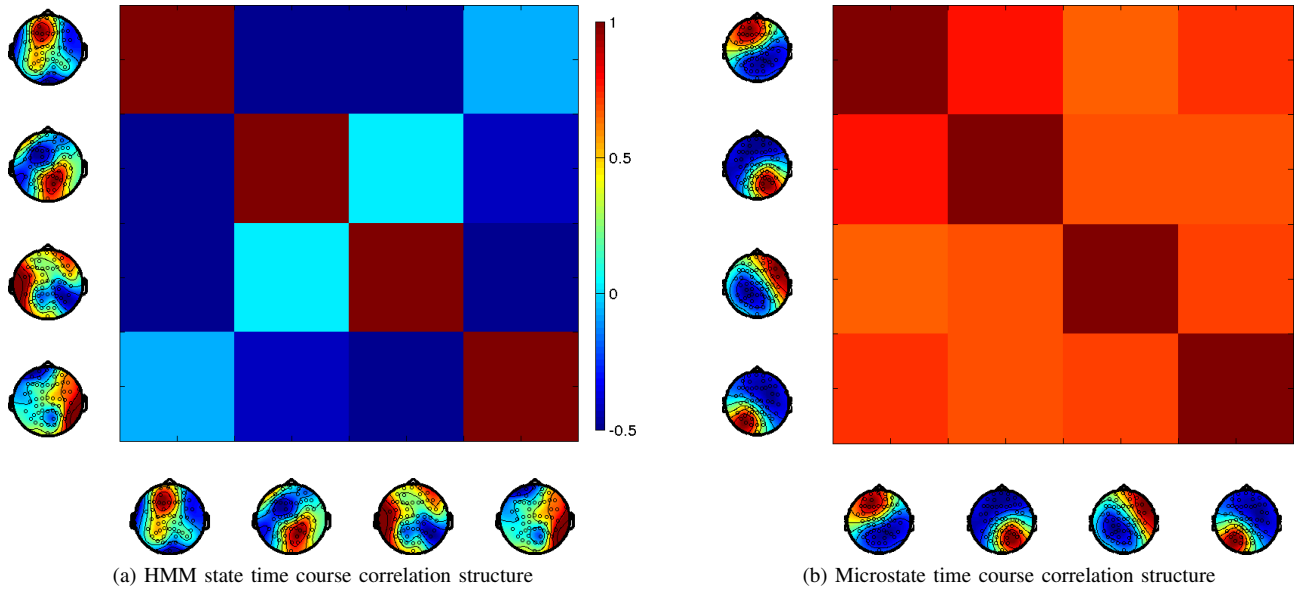


**Fig. 7: Correlation structure of the state time courses for the different modalities** – A strong positive correlation between all EEG microstate time courses is visible, while different HMM state time courses are approximately uncorrelated or negatively correlated.

Notably, the absolute values of the partial correlations are consistently larger by roughly a factor of 2 for the microstates than for the HMM states. This can be explained by the high correlations between the microstate time courses as shown in comparison to the HMM time courses in Fig. 7.

The microstate time courses exhibit pairwise correlations that are consistently larger than 0.6. Conversely the HMM state time courses show correlations down to -0.5. This explains the larger partial partial correlation coefficients in Fig. 6. After regressing out the contribution of time courses that are strongly correlated to the time course of interest the remaining regressor is comparably small and needs therefore larger coefficients to fit the power envelope time courses.

## VII. DISCUSSION AND CONCLUSION

We identified states of quasi-stable topographies in resting state EEG by means of classical microstate analysis and proposed an alternative approach based on a Hidden Markov model with a Gaussian observation model that was tractable for approximate inference using Variational Bayes inference [20]. The microstate analysis identified topographies that are similar to known microstates [24].

Variations in the number of states showed an approximately symmetric splitting of areas of activation (Fig. 11), highlighting the lack of physiological motivation in the microstate procedure. However, this is unsurprising given the algorithm that is based on mere spatial dissimilarity and given the lack of a particular cluster structure as suggested in the plot of the centroid distance as a function of the number of states (Fig. 8).

While the HMM state topographies are less confined, they feature similar activation patterns and can partly be matched to corresponding microstates. This matching was shown to be reflected in the temporal evolution of the state time courses.

Notably the absolute values of these correlations reach their maxima at about 0.4, pointing to a dissimilarity that may correspond to a loss/gain of meaningful information in one of the methods.

The free energy, a measure for the HMM model fitness, decreases steadily for an increase in the number of states for both EEG and MEG data. A possible explanation for the absence of an optimal number of states within the investigated range is the following. For a higher number of states, subject specific activations are introduced in addition to the desirable patterns that are present across subjects. We frequently observe such subject specific states when increasing the number of states (not shown here), particularly in the MEG data. While this was partly amendable by demeaning and variance normalising the subject-wise power envelopes, the reason for this behaviour is likely the acutely distinct covariance structure between subjects. To make the HMM analysis robust and reliable, this issue should be addressed in future work. More generally, a nonparametric model could automatically infer the optimal number of states.

Both, EEG HMM and EEG microstate analysis find dominating state lifetimes of 100–150 ms, which is consistent with earlier findings [41, 19]. However, the EEG microstate duration is usually defined as the time between two GFP peaks with different associated microstate classes. Since the process of switching between states is not limited to the timepoints of local maxima in the GFP, this is likely an overestimate of the true microstate duration as discussed by Gaertner and colleagues. [26]. They proposed a simple stochastic model of the underlying process and estimated true state durations between 10 and 30 ms. This is in disagreement with our empirical results and it remains unclear why the power envelope based HMM approach is not able to capture these dynamics, if they

are present.

Both our approaches show limited consistency of states on a subject level, with the HMM states being distinctly different from most group level states. This poses a limitation for the use of the HMM for between subject comparisons, which could potentially be overcome by defining suitable priors that incorporate between subject similarity.

Further work should also include the investigation of the scaling behaviour of HMM states for both-, EEG and MEG measurements to ascertain whether they exhibit the same scale free behaviour that was found for EEG microstates [14] and that is hypothesized to be necessary for the efficient execution of cognitive processes [42, 43, 44].

Known RNSs were found in the MEG data, by application of the HMM on the parcellated MEG power envelopes. Combined analysis with simultaneously recorded EEG/MEG data confirmed the similarity between microstate and HMM time courses. It provided a richer understanding of the spatial topographies, despite showing little correspondence to known RSNs. However, where present, this correspondence was more pronounced in maps that were derived from EEG HMM states. This can be interpreted as evidence for the hypothesis that EEG HMM states reflect the underlying physiology more accurately than EEG microstates. Additionally, the EEG microstate time courses show strong pairwise temporal correlations, which is not observed for EEG HMM states. While a temporal (and spatial) overlap between RSNs is entirely possible, networks of different function should also be temporally distinct [45]. Thus, a high positive correlation between the dynamics of all given states is unlikely to be a good description of underlying physiology.

Overall our results suggest, that for studies on the group level EEG HMM states could serve as a physiologically motivated alternative to classical EEG microstates. Further work remains to be done to substantiate this proposition and to better understand the relationship between the resting state networks as revealed by simultaneous MEG and EEG.

#### ACKNOWLEDGEMENTS

I would like to thank Markus von Kienlin and Andreas Bruns at Roche for their support and comments. Furthermore, I would like to thank my academic supervisors Mark Woolrich and Steve Smith for their most helpful guidance. I would also like to thank Adam Baker, Andrew Quinn, Giles Coclough and the whole Oxford Centre for Human Brain Activity analysis group for their support and great company.

#### REFERENCES

- [1] Belén Guerra-Carrillo, Allyson P. Mackey, and Silvia A. Bunge. “Resting-state fMRI: a window into human brain plasticity.” eng. In: *Neuroscientist* 20.5 (Oct. 2014), pp. 522–533. DOI: [10.1177/1073858414524442](https://doi.org/10.1177/1073858414524442). URL: <http://dx.doi.org/10.1177/1073858414524442>.
- [2] Nicola Filippini et al. “Distinct patterns of brain activity in young carriers of the APOE-epsilon4 allele.” eng. In: *Proc Natl Acad Sci U S A* 106.17 (Apr. 2009), pp. 7209–7214. DOI: [10.1073/pnas.0811879106](https://doi.org/10.1073/pnas.0811879106). URL: <http://dx.doi.org/10.1073/pnas.0811879106>.
- [3] Maria Centeno and David W. Carmichael. “Network Connectivity in Epilepsy: Resting State fMRI and EEG-fMRI Contributions.” eng. In: *Front Neurol* 5 (2014), p. 93. DOI: [10.3389/fneur.2014.00093](https://doi.org/10.3389/fneur.2014.00093). URL: <http://dx.doi.org/10.3389/fneur.2014.00093>.
- [4] Stefan Lang, Niall Duncan, and Georg Northoff. “Resting-state functional magnetic resonance imaging: review of neurosurgical applications.” eng. In: *Neurosurgery* 74.5 (May 2014), pp. 453–64, 453–64. DOI: [10.1227/NEU.0000000000000307](https://doi.org/10.1227/NEU.0000000000000307). URL: <http://dx.doi.org/10.1227/NEU.0000000000000307>.
- [5] Smadar Ovadia-Caro, Daniel S. Margulies, and Arno Villringer. “The value of resting-state functional magnetic resonance imaging in stroke.” eng. In: *Stroke* 45.9 (Sept. 2014), pp. 2818–2824. DOI: [10.1161/STROKEAHA.114.003689](https://doi.org/10.1161/STROKEAHA.114.003689). URL: <http://dx.doi.org/10.1161/STROKEAHA.114.003689>.
- [6] Christian F Beckmann et al. “Investigations into resting-state connectivity using independent component analysis”. In: *Philosophical Transactions of the Royal Society of London B: Biological Sciences* 360.1457 (2005), pp. 1001–1013. ISSN: 0962-8436. DOI: [10.1098/rstb.2005.1634](https://doi.org/10.1098/rstb.2005.1634).
- [7] J. S. Damoiseaux et al. “Consistent resting-state networks across healthy subjects”. In: *Proceedings of the National Academy of Sciences* 103.37 (2006), pp. 13848–13853. DOI: [10.1073/pnas.0601417103](https://doi.org/10.1073/pnas.0601417103). URL: <http://www.pnas.org/content/103/37/13848.abstract>.
- [8] Michel. *Electrical Neuroimaging (Cambridge Medicine)*. July 2009. URL: <http://amazon.com/o/ASIN/B002SEKZ4M/>.
- [9] Malcolm Proudfoot et al. “Magnetoencephalography.” eng. In: *Pract Neurol* 14.5 (Oct. 2014), pp. 336–343. DOI: [10.1136/practneurol-2013-000768](https://doi.org/10.1136/practneurol-2013-000768).
- [10] Biyu J. He et al. “Electrophysiological correlates of the brain’s intrinsic large-scale functional architecture”. In: *Proceedings of the National Academy of Sciences* 105.41 (2008), pp. 16039–16044. DOI: [10.1073/pnas.0807010105](https://doi.org/10.1073/pnas.0807010105). URL: <http://www.pnas.org/content/105/41/16039.abstract>.
- [11] Zhongming Liu et al. “Large-scale spontaneous fluctuations and correlations in brain electrical activity observed with magnetoencephalography”. In: *NeuroImage* 51.1 (2010), pp. 102–111. ISSN: 1053-8119. DOI: [10.1016/j.neuroimage.2010.01.092](https://doi.org/10.1016/j.neuroimage.2010.01.092). URL: <http://www.sciencedirect.com/science/article/pii/S1053811910001151>.
- [12] K. Linkenkaer-Hansen et al. “Long-range temporal correlations and scaling behavior in human brain oscillations.” eng. In: *J Neurosci* 21.4 (Feb. 2001), pp. 1370–1377.
- [13] Manfred G. Kitzbichler et al. “Broadband criticality of human brain network synchronization.” eng. In: *PLoS Comput Biol* 5.3 (Mar. 2009), e1000314. DOI: [10.1371/journal.pcbi.1000314](https://doi.org/10.1371/journal.pcbi.1000314).
- [14] Dimitri Van de Ville, Juliane Britz, and Christoph M. Michel. “EEG microstate sequences in healthy humans

- at rest reveal scale-free dynamics.” eng. In: *Proc Natl Acad Sci U S A* 107.42 (Oct. 2010), pp. 18179–18184. DOI: [10.1073/pnas.1007841107](https://doi.org/10.1073/pnas.1007841107). URL: <http://dx.doi.org/10.1073/pnas.1007841107>.
- [15] Mark Woolrich et al. “{MEG} beamforming using Bayesian {PCA} for adaptive data covariance matrix regularization”. In: *NeuroImage* 57.4 (2011), pp. 1466–1479. ISSN: 1053-8119. DOI: [http://dx.doi.org/10.1016/j.neuroimage.2011.04.041](https://doi.org/10.1016/j.neuroimage.2011.04.041). URL: <http://www.sciencedirect.com/science/article/pii/S105381191100440X>.
- [16] Mark W. Woolrich et al. “Dynamic state allocation for MEG source reconstruction.” eng. In: *NeuroImage* 77 (Aug. 2013), pp. 77–92. DOI: [10.1016/j.neuroimage.2013.03.036](https://doi.org/10.1016/j.neuroimage.2013.03.036).
- [17] Nela Cicmil et al. “Localization of MEG human brain responses to retinotopic visual stimuli with contrasting source reconstruction approaches.” eng. In: *Front Neurosci* 8 (2014), p. 127. DOI: [10.3389/fnins.2014.00127](https://doi.org/10.3389/fnins.2014.00127). URL: <http://dx.doi.org/10.3389/fnins.2014.00127>.
- [18] I. Rezek and S. J. Roberts. “Ensemble hidden Markov models for biosignal analysis”. In: *Digital Signal Processing, 2002. DSP 2002. 2002 14<sup>th</sup> International Conference on*. Vol. 1. 2002, pp. 387–391. DOI: [10.1109/ICDSP.2002.1027907](https://doi.org/10.1109/ICDSP.2002.1027907). URL: <http://ieeexplore.ieee.org/stamp/stamp.jsp?arnumber=1027907>.
- [19] Adam P. Baker et al. “Fast transient networks in spontaneous human brain activity.” eng. In: *Elife* 3 (2014), e01867. DOI: [10.7554/eLife.01867](https://doi.org/10.7554/eLife.01867).
- [20] Diego Vidaurre et al. “Spectrally resolved fast transient brain states in electrophysiological data”. In Preparation.
- [21] T. Koenig et al. “A deviant EEG brain microstate in acute, neuroleptic-naïve schizophrenics at rest”. English. In: *European Archives of Psychiatry and Clinical Neuroscience* 249.4 (1999), pp. 205–211. ISSN: 0940-1334. DOI: [10.1007/s004060050088](https://doi.org/10.1007/s004060050088). URL: <http://dx.doi.org/10.1007/s004060050088>.
- [22] Thomas Koenig et al. “Millisecond by millisecond, year by year: normative EEG microstates and developmental stages.” eng. In: *NeuroImage* 16.1 (May 2002), pp. 41–48. DOI: [10.1006/nimg.2002.1070](https://doi.org/10.1006/nimg.2002.1070).
- [23] D. Lehmann, R. D. Pascual-Marqui, and C. Michel. “EEG microstates”. In: 4.3 (2009). revision 88985, p. 7632.
- [24] Arjun Khanna et al. “Microstates in resting-state EEG: current status and future directions.” eng. In: *Neurosci Biobehav Rev* 49 (Feb. 2015), pp. 105–113. DOI: [10.1016/j.neubiorev.2014.12.010](https://doi.org/10.1016/j.neubiorev.2014.12.010). URL: <http://dx.doi.org/10.1016/j.neubiorev.2014.12.010>.
- [25] T Koenig et al. “Brain connectivity at different time-scales measured with EEG”. In: *Philosophical Transactions of the Royal Society of London B: Biological Sciences* 360.1457 (2005), pp. 1015–1024. ISSN: 0962-8436. DOI: [10.1098/rstb.2005.1649](https://doi.org/10.1098/rstb.2005.1649).
- [26] Matthias Gärtnner et al. “A stochastic model for EEG microstate sequence analysis.” eng. In: *NeuroImage* 104 (Jan. 2015), pp. 199–208. DOI: [10.1016/j.neuroimage.2014.10.014](https://doi.org/10.1016/j.neuroimage.2014.10.014). URL: <http://dx.doi.org/10.1016/j.neuroimage.2014.10.014>.
- [27] R. D. Pascual-Marqui, C. M. Michel, and D. Lehmann. “Segmentation of brain electrical activity into microstates: model estimation and validation.” eng. In: *IEEE Trans Biomed Eng* 42.7 (July 1995), pp. 658–665. DOI: [10.1109/10.391164](https://doi.org/10.1109/10.391164). URL: <http://dx.doi.org/10.1109/10.391164>.
- [28] Robert Tibshirani and Guenther Walther. “Cluster Validation by Prediction Strength”. In: *Journal of Computational and Graphical Statistics* 14.3 (2005), pp. 511–528. DOI: [10.1198/106186005X59243](https://doi.org/10.1198/106186005X59243). URL: <http://dx.doi.org/10.1198/106186005X59243>.
- [29] Han Yuan et al. “Spatiotemporal dynamics of the brain at rest—exploring EEG microstates as electrophysiological signatures of BOLD resting state networks.” eng. In: *NeuroImage* 60.4 (May 2012), pp. 2062–2072. DOI: [10.1016/j.neuroimage.2012.02.031](https://doi.org/10.1016/j.neuroimage.2012.02.031). URL: <http://dx.doi.org/10.1016/j.neuroimage.2012.02.031>.
- [30] Verena Brodbeck et al. “EEG microstates of wakefulness and NREM sleep.” eng. In: *NeuroImage* 62.3 (Sept. 2012), pp. 2129–2139. DOI: [10.1016/j.neuroimage.2012.05.060](https://doi.org/10.1016/j.neuroimage.2012.05.060). URL: <http://dx.doi.org/10.1016/j.neuroimage.2012.05.060>.
- [31] Dietrich Lehmann et al. “EEG microstate duration and syntax in acute, medication-naïve, first-episode schizophrenia: a multi-center study.” eng. In: *Psychiatry Res* 138.2 (Feb. 2005), pp. 141–156. DOI: [10.1016/j.psychresns.2004.05.007](https://doi.org/10.1016/j.psychresns.2004.05.007). URL: <http://dx.doi.org/10.1016/j.psychresns.2004.05.007>.
- [32] Keiichiro Nishida et al. “EEG microstates associated with salience and frontoparietal networks in frontotemporal dementia, schizophrenia and Alzheimer’s disease.” eng. In: *Clin Neurophysiol* 124.6 (June 2013), pp. 1106–1114. DOI: [10.1016/j.clinph.2013.01.005](https://doi.org/10.1016/j.clinph.2013.01.005). URL: <http://dx.doi.org/10.1016/j.clinph.2013.01.005>.
- [33] Drausin F. Wulsin, Emily B. Fox, and Brian Litt. “Parsing epileptic events using a Markov switching process model for correlated time series Supplementary Materials”. In: *JMLR* 28.1 (2013), pp. 356–364.
- [34] D. Mantini et al. “Electrophysiological signatures of resting state networks in the human brain.” eng. In: *Proc Natl Acad Sci U S A* 104.32 (Aug. 2007), pp. 13170–13175. DOI: [10.1073/pnas.0700668104](https://doi.org/10.1073/pnas.0700668104). URL: <http://dx.doi.org/10.1073/pnas.0700668104>.
- [35] Juliane Britz, Dimitri Van De Ville, and Christoph M. Michel. “BOLD correlates of EEG topography reveal rapid resting-state network dynamics.” eng. In: *NeuroImage* 52.4 (Oct. 2010), pp. 1162–1170. DOI: [10.1016/j.neuroimage.2010.02.052](https://doi.org/10.1016/j.neuroimage.2010.02.052). URL: <http://dx.doi.org/10.1016/j.neuroimage.2010.02.052>.
- [36] Joerg F. Hipp and Markus Siegel. “BOLD fMRI Correlation Reflects Frequency-Specific Neuronal Correlation.” eng. In: *Curr Biol* 25.10 (May 2015), pp. 1368–1374. DOI: [10.1016/j.cub.2015.03.049](https://doi.org/10.1016/j.cub.2015.03.049). URL: <http://dx.doi.org/10.1016/j.cub.2015.03.049>.

- [37] Harumi Yoshinaga et al. “Benefit of simultaneous recording of EEG and MEG in dipole localization.” eng. In: *Epilepsia* 43.8 (Aug. 2002), pp. 924–928.
- [38] S. Knake et al. “The value of multichannel MEG and EEG in the presurgical evaluation of 70 epilepsy patients.” eng. In: *Epilepsy Res* 69.1 (Apr. 2006), pp. 80–86. DOI: [10.1016/j.eplepsyres.2006.01.001](https://doi.org/10.1016/j.eplepsyres.2006.01.001). URL: <http://dx.doi.org/10.1016/j.eplepsyres.2006.01.001>.
- [39] B. D. Van Veen et al. “Localization of brain electrical activity via linearly constrained minimum variance spatial filtering.” eng. In: *IEEE Trans Biomed Eng* 44.9 (Sept. 1997), pp. 867–880. DOI: [10.1109/10.623056](https://doi.org/10.1109/10.623056). URL: <http://dx.doi.org/10.1109/10.623056>.
- [40] Christopher M. Bishop. *Pattern Recognition and Machine Learning*. 1st Edition. Springer, 2013. ISBN: 9788132209065. URL: <http://amazon.com/o/ASIN/8132209060/>.
- [41] D. Lehmann, H. Ozaki, and I. Pal. “EEG alpha map series: brain micro-states by space-oriented adaptive segmentation.” eng. In: *Electroencephalogr Clin Neurophysiol* 67.3 (Sept. 1987), pp. 271–288.
- [42] Dante R. Chialvo. “Critical brain networks”. In: *Physica A* 340 (2008), :756(2004).
- [43] Ariel Haimovici et al. “Brain Organization into Resting State Networks Emerges at Criticality on a Model of the Human Connectome”. In: *Phys. Rev. Lett.* 110 (17 Apr. 2013), p. 178101. DOI: [10.1103/PhysRevLett.110.178101](https://doi.org/10.1103/PhysRevLett.110.178101).
- [44] Enzo Tagliazucchi et al. “Criticality in large-scale brain fMRI dynamics unveiled by a novel point process analysis.” In: *Frontiers in Physiology* 3.15 (2012). ISSN: 1664-042X. DOI: [10.3389/fphys.2012.00015](https://doi.org/10.3389/fphys.2012.00015).
- [45] Stephen M. Smith et al. “Temporally-independent functional modes of spontaneous brain activity”. In: *Proceedings of the National Academy of Sciences* 109.8 (2012), pp. 3131–3136. DOI: [10.1073/pnas.1121329109](https://doi.org/10.1073/pnas.1121329109). URL: <http://www.pnas.org/content/109/8/3131.abstract>.

APPENDIX  
SUPPLEMENTARY FIGURES

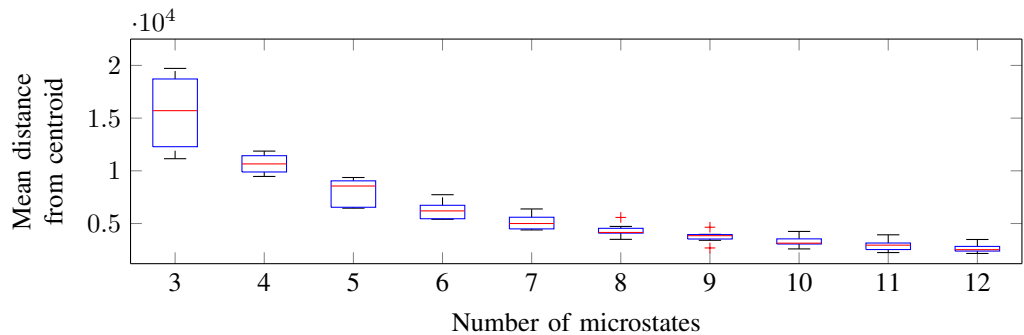


Fig. 8: **Microstate clustering** – The mean distance of all topographies from their corresponding cluster centroid is shown as a function of the number of clusters. Boxplots depict the variation across the different clusters.

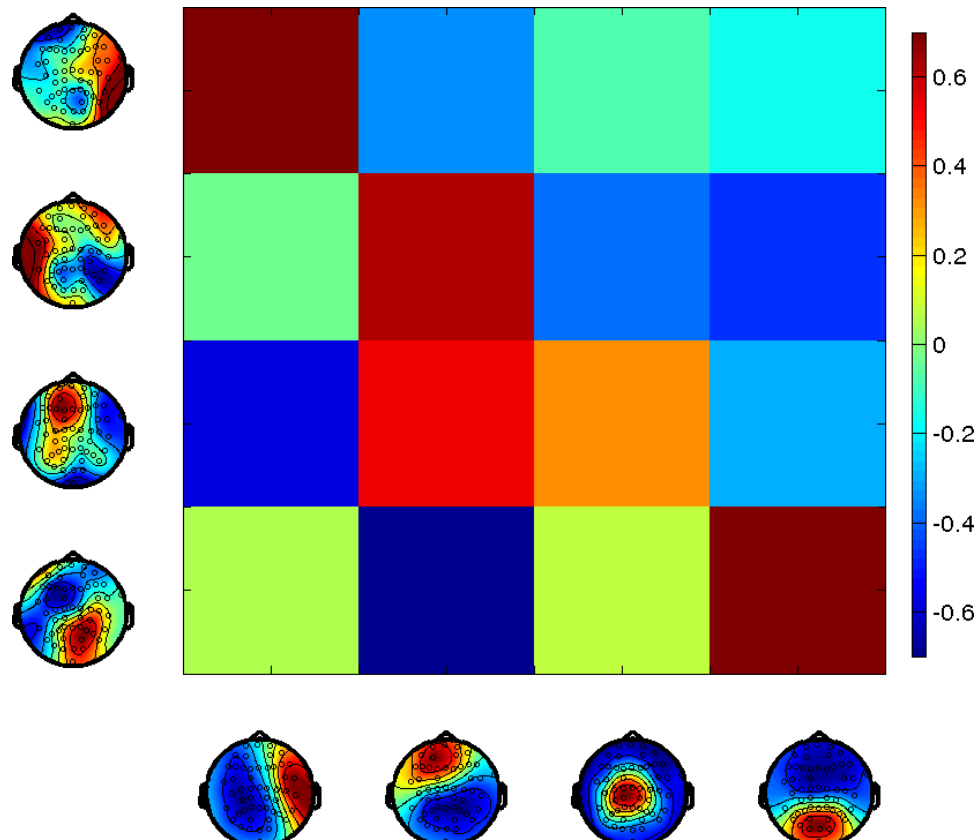


Fig. 9: **Correlation structure of microstate and HMM state spatial maps** – Compare to the temporal correlations in Fig. 4.

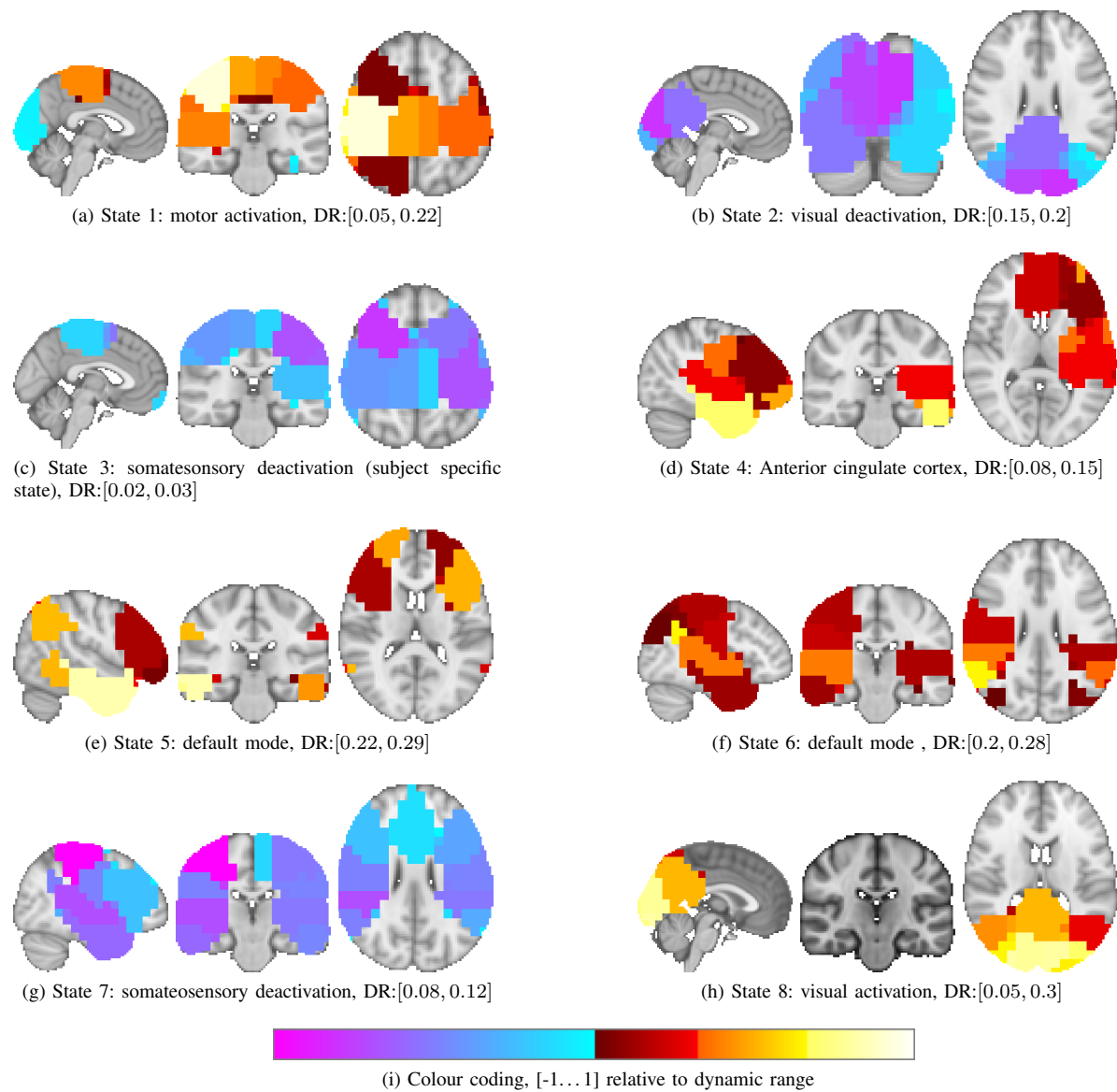
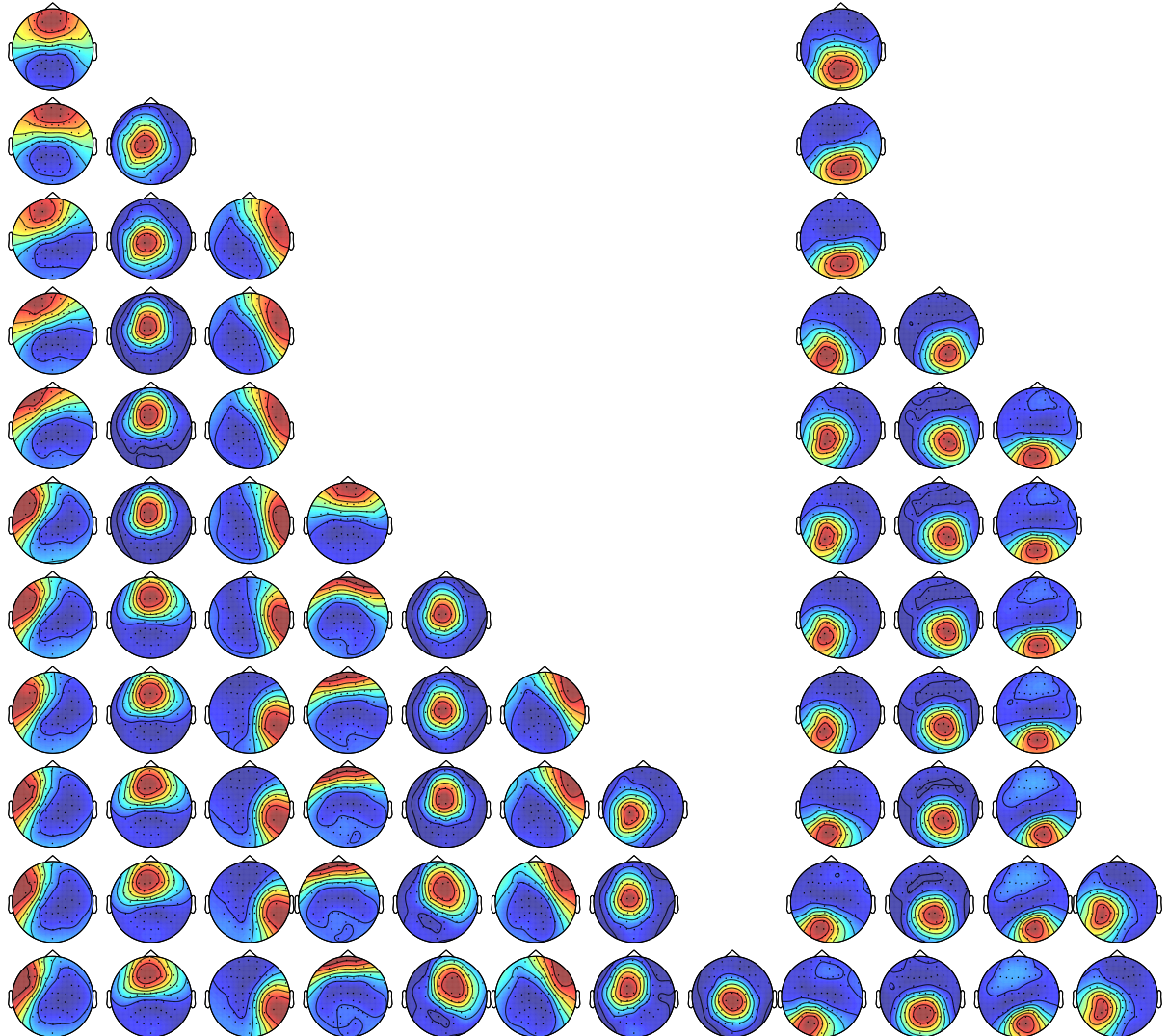


Fig. 10: **MEG HMM states** – States are inferred based on parcellated envelope data.



**Fig. 11: Microstate topographies** – The microstate procedure was carried out for fixed numbers of clusters ( $k = 1..12$ ). The states are depicted to highlight how clusters split, when additional clusters are introduced. The colour coding is normalised for every topography, in order to facilitate the comparison between states and modalities.

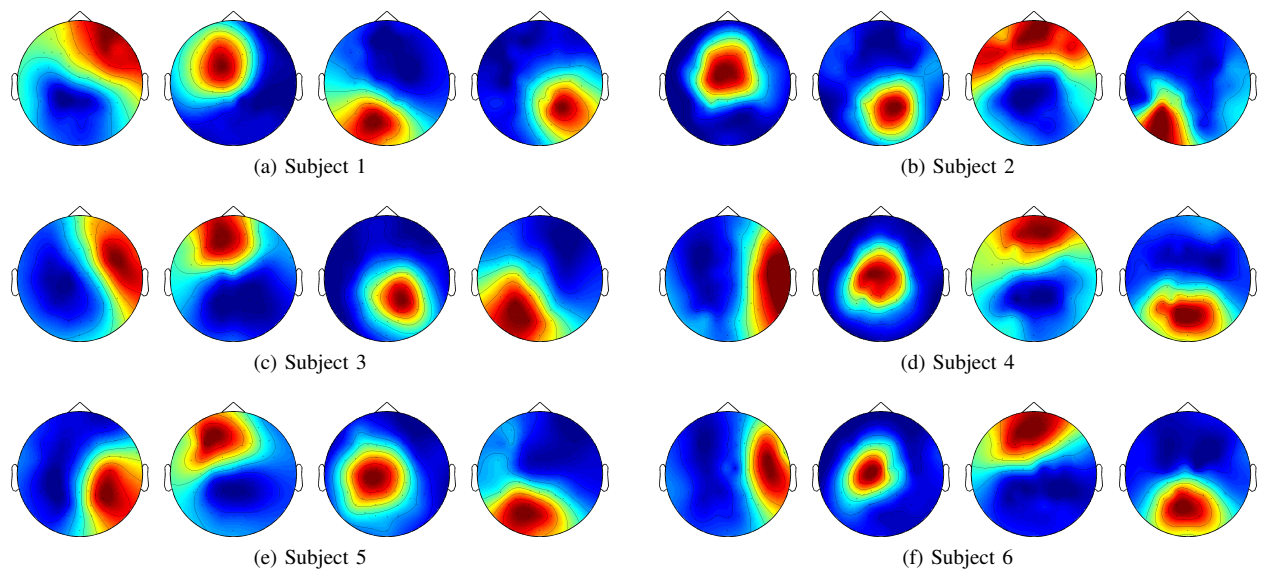


Fig. 12: **Subject-wise microstate topographies** – The colour coding is normalised for every topography. Compare to the group topographies in Fig. 2.

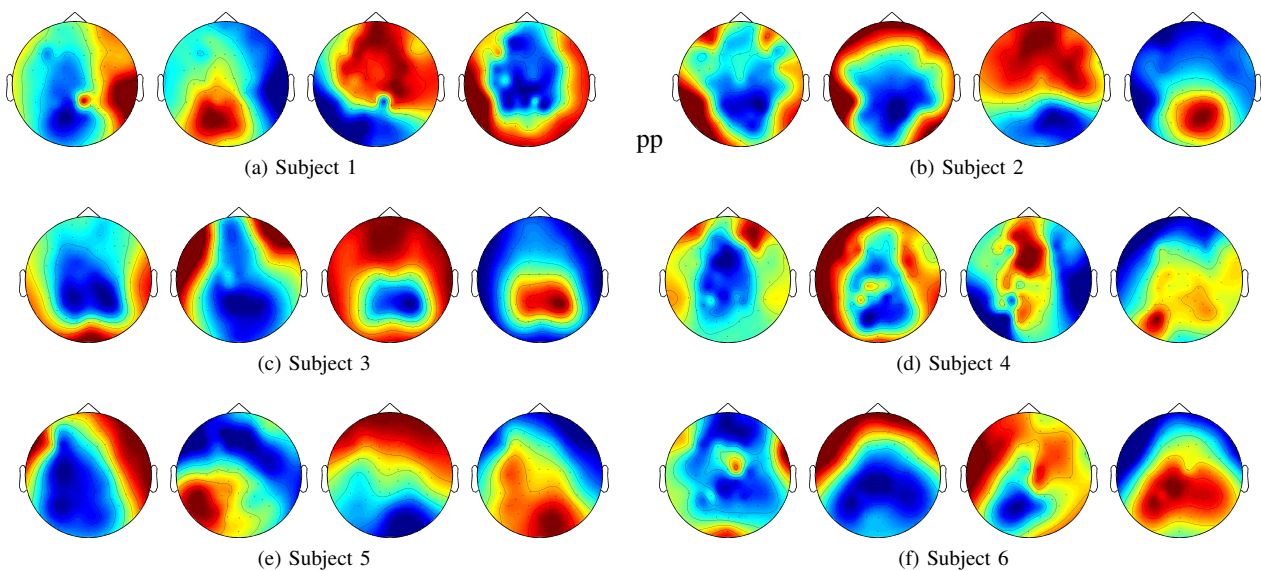


Fig. 13: **Subject-wise HMM topographies** – The colour coding is normalised for every topography. Compare to the group topographies in Fig. 2.